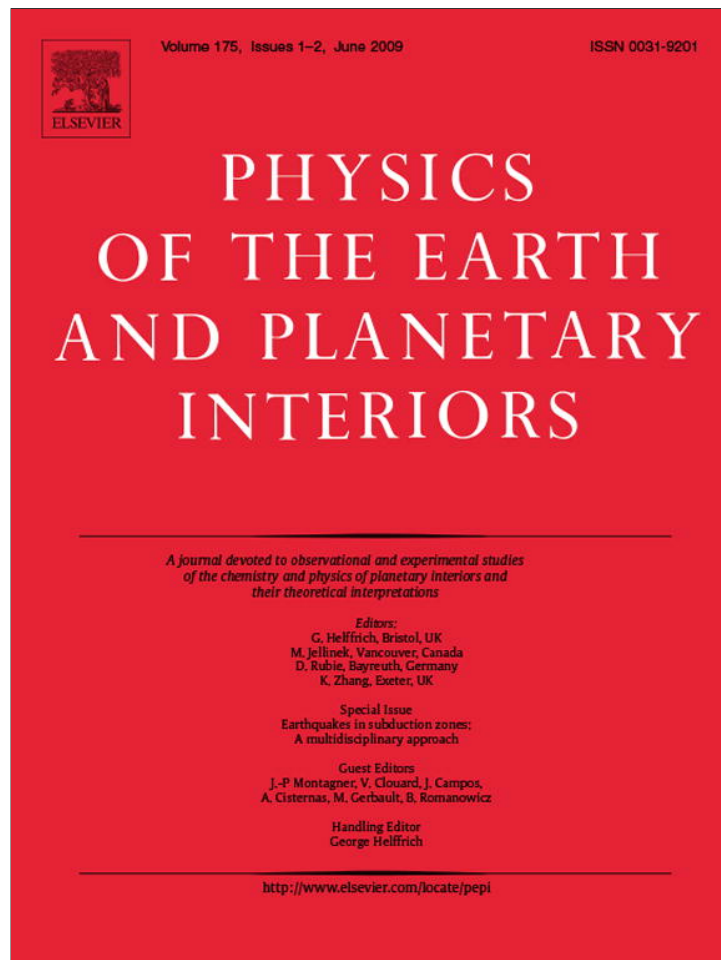


Provided for non-commercial research and education use.
Not for reproduction, distribution or commercial use.



This article appeared in a journal published by Elsevier. The attached copy is furnished to the author for internal non-commercial research and education use, including for instruction at the authors institution and sharing with colleagues.

Other uses, including reproduction and distribution, or selling or licensing copies, or posting to personal, institutional or third party websites are prohibited.

In most cases authors are permitted to post their version of the article (e.g. in Word or Tex form) to their personal website or institutional repository. Authors requiring further information regarding Elsevier's archiving and manuscript policies are encouraged to visit:

<http://www.elsevier.com/copyright>



Contents lists available at ScienceDirect

Physics of the Earth and Planetary Interiors

journal homepage: www.elsevier.com/locate/pepi

Upper plate deformation measured by GPS in the Coquimbo Gap, Chile

Christophe Vigny^{a,*}, Alain Rudloff^a, Jean-Claude Ruegg^b, Raul Madariaga^a, Jaime Campos^c, Manuel Alvarez^c^a Laboratoire de Géologie, Ecole Normale Supérieure (ENS), CNRS, Paris, France^b Institut de Physique du Globe (IPGP), Paris, France^c Departamento de Geofísica (DGF), Universidad de Chile, Santiago, Chile

ARTICLE INFO

Article history:

Received 29 March 2007

Accepted 29 February 2008

Keywords:

GPS

Tectonics

Seismicity

Subduction

Transient

ABSTRACT

Since the $M_w=7.3$ Punitaqui earthquake in 1997, the area between 30°S and 32°S (Coquimbo–Illapel section) of the Chilean subduction has been the locus of a decennial seismic swarm. A dense network of 30+ benchmarks have been installed in this area and surveyed six times with high precision GPS over the last 3 years. Surface deformation here is compatible with elastic loading due to partial locking on the subduction interface at depth. Here we show that in this area, only 40–45% of the total convergence rate between Nazca and South America plates gives way to accumulation of elastic deformation in the upper plate, the remaining 60–55% being dissipated by free or aseismic slip, the cumulative slip due to the seismic swarm explaining no more than 1/3rd to 1/4th of it. We also find that the accumulation decreases northward, to reach almost zero around 30°S (La Serena – Tongoy). Whether this is a steady state or only a transient pattern (a steady decrease of coupling) is not clear since our measurements span only 3 years and since early measurements 10 years ago were sparse and differ only marginally from ours.

© 2009 Elsevier B.V. All rights reserved.

1. Introduction

The Chilean subduction has one of the highest levels of seismic activity in the world, with a large earthquake of $M_w > 8$ every 5–10 years. These events are the consequence of subduction of the Nazca plate beneath South America at a convergence rate as high as 8 cm/yr in the N 78°E direction (DeMets et al., 1990, 1994). In Chile, several studies have shown an along strike variation in the dip angle of the slab, and possible segmentation of the subduction zone, well expressed in the surface geology and morphology (Barazangi and Isacks, 1976). The fast convergence is accommodated by large inter- and intra-plate earthquakes, and by shallow earthquakes associated with intra-continental fault systems in the Andes cordillera and the Altiplano-Puna. The study of Chilean earthquakes has a long history and major seismic gaps, e.g. Central Chile (Constitución–Concepción $35\text{--}37^\circ\text{S}$) and North Chile (Antofagasta–Arica $18\text{--}27^\circ\text{S}$), are reaching the end of the seismic cycle with a high megathrust earthquake risk in the 21st century (Kelleher, 1972; Nishenko, 1985). Unfortunately, the identification of these gaps does not solve the medium term prediction problem due to the space and time variability of the seismic activity which often occurs in swarms, whose origin remains to be elucidated.

The Coquimbo–Illapel area ($30\text{--}32^\circ\text{S}$) of the Coquimbo region of North central Chile was the site of major earthquakes in 1730, 1880 and 1943 (Nishenko, 1985; Beck et al., 1998). The last major event in this area occurred on 15 October 1997 at a depth of 55 km under the city of Punitaqui. This unusual slab–push event of $M_w 7.3$ was studied in detail by Lemoine et al. (2001). Several seismological studies have been devoted to delimit the structures and the geometry of the subduction zone of the Coquimbo region (Pardo et al., 2002a,b). It is presently the place of a remarkable seismic activity that started in 1997 a few months earlier than the Punitaqui earthquake. As shown by Gardi et al. (2006) the seismicity of the inter-plate zone westward of the 1997 Punitaqui earthquake has been the site of increased seismicity since July 1997 when a series of four shallow events of $M_w > 6$ occurred in the inter-plate zone near 30.5°S . The increased seismicity appears to continue uninterrupted until at least last October when an earthquake of $M_w 6.2$ took place in the area. Simple stress transfer modelling indicates that aseismic slip can explain this sequence (Gardi et al., 2006). This puzzling seismicity (which could in fact have started as early as 1992) could be either the herald of a major earthquake initiation and/or the manifestation of slow aseismic transient slip on the subduction interface. Finally, early (1994–1996) GPS measurements in the area clearly show at least one anomalous velocity at Tongoy (TONG – 30.2°S) (Klotz et al., 2001). Although it is on the coast, this point shows less Eastward deformation than points further away from the trench. In other words, at the time of the measurements, this area was moving away from the central valley

* Corresponding author.

E-mail address: vigny@mailhost.geologie.ens.fr (C. Vigny).

and towards the trench relatively speaking. It is possible that this point was responding to slow/transient motions on the subduction interface.

In order to investigate in details the current deformation of the Coquimbo region, we established a small scale GPS network of 30+ benchmarks between 30°S and 32°S with an average distance between stations of less than 30 km. This mesh was designed to render the network sensitive to transient slips taking place on the subduction interface and possibly at the initiation of the transition depth between locked and freely slipping slab. We measure this network as frequently as possible (every 6 months) to monitor long term variations of the coupling on the interface.

2. Seismicity of Coquimbo

The Coquimbo area shows signs of increased seismic activity, or accelerated moment release as described, among others, by Mignan et al. (2006). Unfortunately, we do not have a sufficiently long catalog of seismicity in order to formally test the hypotheses. We have examined three catalogs of central Chile seismicity, from the National Earthquake Information Center (NEIC, 2006), International Seismological Center (ISC, 2001) and the centennial catalog (Engdahl and Villaseñor, 2002). After examining the completeness of the catalogs using standard techniques, we concluded that we could only use the centennial catalog that contains earthquakes of magnitude greater than 5.5 in the region, but is not enough to test for changes in seismicity rate. Finally, we decided to use the ISC catalog for the period 1990–2005. This catalog is complete from magnitude 4.5, except for a period of transition between 1990 and 1992 when the University of Chile started reporting local magnitudes for all earthquakes in the region. Although not all events are well located, the catalog appears to be uniform and therefore we can verify the observation by Gardi et al. (2006) who used the NEIC catalog to demonstrate an acceleration of seismicity that started in July 1997, when a series of six shallow thrust events occurred on the plate interface in the region from 30.5°S to 31.5°S. After a pause of about 2 months from July to October, seismicity moved inland and culminated in a large $M_w = 7.3$ earthquake on 15 October 1997. This event was a very rare slab-push (compression along the slab) event that took place inside the downgoing slab near the transition zone from locked to continuous slip. Gardi et al. (2006) proposed

that this event was due to a tear in the slab due to the strong accumulation of stresses in the transition zone from continuous slip to the seismogenic interface.

Fig. 1 shows the seismicity of the region from 28°S to 32°S in the period 1992–1997 and after the 1997 events. While seismicity in the region from 30°S to 31°S was weak in the initial period it has been quite strong since 1997, with 12 events of $M_w > 6$. The zone from 30°S to 31°S is situated very close to the epicentral area of the 1946 earthquake as relocated by Engdahl et al. in the centennial catalog. This event of $M_w = 7.9$ and $M_o = 6 \times 10^{20}$ N m was studied in detail by Beck et al. (1998). The seismicity of 1997 started very close to the epicentral area of 1946 and it is possible that it represents early foreshocks of a future event in the area. If the inter-plate zone were fully locked, as proposed by Khazaradze and Klotz, 2003, the slip deficit in the locked interface would be of the order of 4 m (60 years at 6.5 cm/yr) and we would be close to rupture in about 10 years if the next earthquake is similar to that of 1943. It is therefore very important to study the current slip at the plate interface in order to determine whether the plate interface is fully locked or not and, in the latter case whether slip in the interseismic period is continuous or episodic.

In Fig. 2, we show the rate of seismicity along the plate interface according to the ISC catalog. As in most studies of accelerating moment release we plot the cumulative number of events in the ISC catalog in the area as a function of time. We did also compute the cumulative magnitude to test whether there are differences. If seismicity follows the Gutenberg Richter relation both curves should be homothetic, as is actually the case in Fig. 2. We clearly observe that after the 1997 events in the plate interface and inside the slab, seismicity made a fast jump and then decreased to reach an almost steady state regime after mid-1998. This initial response follows, as expected, the classical Omori law. After mid-1998, the seismicity rate settles to a value that is significantly larger than that before the 1997 events. There is clear evidence of a change in seismic moment release rate, but we cannot resolve an increase in seismicity rate near the end of the catalog at about 2005. Thus, our temporary conclusion is that seismicity in Coquimbo underwent a change in regime around mid-1997 and has remained at a sustained high rate. We also computed the cumulative slip on the interface since 1985, using the earthquakes which clearly take place on the subduction plane (Fig. 2). We reach the conclusion that the cumu-

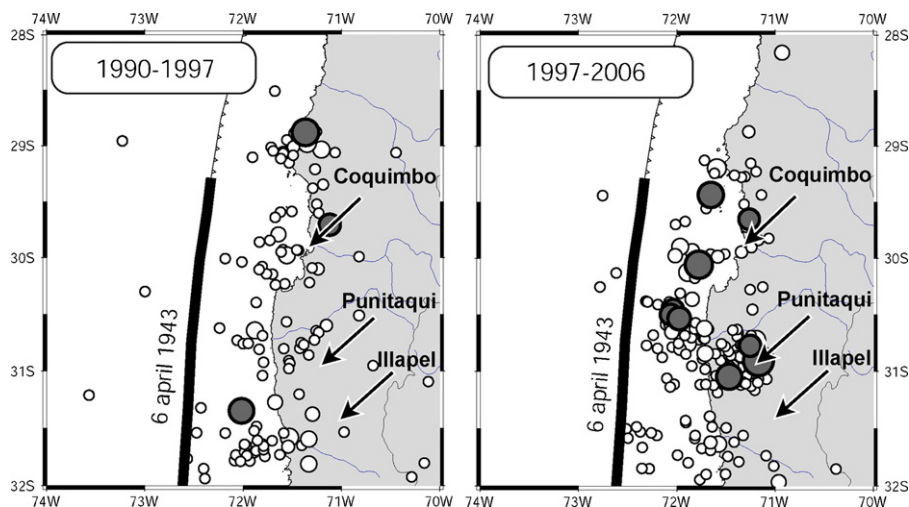


Fig. 1. Seismicity of the Coquimbo area from the ISC catalog for the period 1990–2007. On the left the map shows the seismicity from 1990 to 1997 just before the events of Coquimbo and the Punitaqui intermediate depth event. Along the trench we plot the approximate rupture area of the 1943 earthquake (Beck et al., 1998). On the right we show the seismicity since the 1997 events. Events larger than $M_w 6$, shown in lighter color, were extracted from the Centennial catalog of Engdahl and Villaseñor (2002), the rest of the seismicity is from the ISC catalog. We observe that since 1997 the region around the Punitaqui earthquake has been very active.

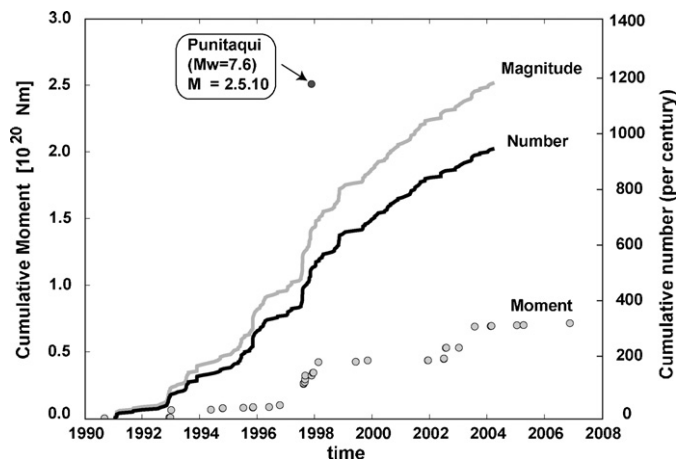


Fig. 2. Seismicity rate and cumulative co-seismic moment in the Coquimbo area since 1992. Shaded curves show the cumulative number of earthquakes (black) and cumulative magnitude (grey) from ISC catalog. We observe a clear aftershock sequence from mid-1997 to mid-1998. This sequence satisfies Omori's law and then seismicity settles to a higher level than before the 1997 events. A small, but not well resolved, acceleration in seismicity rate appears to be occurring in the last couple of years before 2005, but the ISC catalog is not complete yet after October 2004. Grey circles show the cumulative co-seismic moment due to the larger earthquakes occurring on the subduction interface. An equivalent moment of 0.8×10^{20} N m ($M_w \sim 7.2$) is reached after 15 years. Punitaqui intra-plate earthquake moment (2.5×10^{20} N m) is shown for comparison (black circle).

lative co-seismic slip on the whole segment over the last 10 years is equivalent to a magnitude 7.2 earthquake.

3. GPS data analysis

As part of a joint Chilean-French cooperation project, 20 new benchmarks were installed in the Coquimbo gap (between 30°S and 32°S) in April 2004. Two additional benchmarks were deployed in December 2004 and three more in May 2006. Our network also includes pre-existing markers in this area: six from the South American Geodynamic Activities (SAGA) project (Klotz et al., 2001; Khazaradze and Klotz, 2003) and two from the Central Andes Project (CAP) (Kendrick et al., 2001), bringing the total number of repeatedly measured sites to 33. Apart from the CAP sites (and one broken SAGA marker), all other sites are equipped with specially designed bolts sealed in bedrock outcrops. These sites enable direct antenna centering with sub-millimeter accuracy. This network has been surveyed six times in May and December 2004, 2005 and 2006. All sites were measured using a single type of Ashtech ZX-treme dual-frequency receivers equipped with the same kind of antennae (Ashtech Geodetic IV). During all campaigns, four points (LVIL and SLMC in the south and OVLL and TOLO in the north) were measured continuously in 24-h sessions. Other sites were measured for 12–24 h per day over 3–7 days.

We reduce these data in 24-h sessions to daily estimates of station positions using the GAMIT software (King and Bock, 2000), choosing the ionosphere-free combination, and fixing the ambiguities to integer values. We use precise orbits from the International GNSS Service for Geodynamics (IGS) (Beutler et al., 1993). We also use IGS Tables to describe the phase centers of the antennae. We

Table 1
Average short (<300 km) baseline repeatabilities (root mean square scatter about the mean) for each of the six campaigns.

	April 2004	December 2004	April 2005	December 2005	April 2006	November 2006
North rep	1.3	1.9	1.2	1.4	0.8	1.6
East rep.	2.3	2.8	2.5	2.2	1.3	2.5
Vertical rep.	4.6	5.8	4.3	5.0	3.5	4.8

Values are in mm.

estimate one tropospheric vertical delay parameter per station every 3 h. The horizontal components of the calculated relative position vectors are precise to within a few millimeters for pairs of stations less than 300 km apart, as measured by the root mean square (RMS) scatter about the mean (so-called baseline repeatability) (Table 1).

In the second step, we combine the daily solutions using the GLOBK software (Herring et al., 1990) in a “regional stabilization” approach. To define a consistent reference frame for all epochs, we include tracking data from a selection of permanent stations (19) in South America, some of them belonging to the IGS (Neilan, 1995). Seven stations are within or very close to the deformation area, 10 more span the South-American craton in Brazil, Guyana and Argentina, and the remaining two samples the Nazca plate. We combine daily solutions using Helmert-like transformations to estimate translation, rotation, scale and Earth orientation parameters (polar motion and UT1 rotation). This “stabilization” procedure defines a reference frame by minimizing, in the least-square sense, the departure from the prior values determined in the International Terrestrial Reference Frame (ITRF) 2000 (Altamimi et al., 2002). This procedure estimates the positions and velocities for a set of eight well-determined stations in and around our study area (BRAZ, FORT, KOUR, LPSG, RIOG, SANT, ISPA, GLPS). The misfit to these “stabilization” stations is 1.3 mm in position and 0.7 mm/yr in velocity.

4. Horizontal velocities

This procedure leads to horizontal velocities with respect to ITRF2000 (Table 2). We compute velocities relative to the South-American plate by using the angular velocity of this plate (25.4°S, 124.6°W, 0.11°/Myr) given by the NNR-Nuvel-1A model (DeMets et al., 1994). In this reference frame, six sites located far from the subduction zone and supposedly on the South-American plate, show velocities smaller than 1 mm/yr with no systematic trend, and especially at the latitude of our network (Fig. 3, Table 2). Trying to invert for a plate angular velocity using those station velocities in ITRF2000, we find (23.2°S, 121.6°W, 0.127°/Myr). In this South America plate motion determined by GPS, station velocities differ by no more than 1 mm/yr with respect to those of the NNR-Nuvel-1A. We consider this difference not very significant. Therefore, we conclude that the South-American Craton is not affected by internal deformation (at least by no more than 1 mm/yr) and that its present day angular velocity determined here does not differ significantly from its long term (3 Ma) average determined in the NNR-Nuvel-1A model (again at least by no more than 1 mm/yr). For this reason, we decided to plot all GPS velocities relatively to the well-known NNR-Nuvel-1A South America plate, rather than any available geodetically determined South America (i.e. ITRF2000 or ITRF2005). In any case, the difference is at the 1 mm/yr level and can only be investigated with long and extremely precise time series of stations well spread over the whole plate, which is not the case in this study.

4.1. Far-field velocities

In this South-American-fixed reference frame, the velocity at Easter Island (ISPA) is 68 mm/yr (± 1 mm/yr at 3- σ), oriented

Table 2
Site positions and velocities, in ITRF2000 and relative to South-America plate.

SITE	Position		Velocity/ITRF2000		Velocity/S.A.		Uncertainties		Correlation
	Lon	Lat	Vlon	Vlat	Vlon	Vlat	σ Vlon	σ Vlat	
AGUA ^a	289.193	-30.982	21.9	15.8	23.0	6.9	3.9	3.0	0.008
ANDA	288.930	-30.278	16.3	18.6	17.5	9.7	1.5	1.4	0.000
BRAZ ^b	312.122	-15.947	-3.8	10.9	0.6	0.1	1.3	1.2	-0.011
BSJL	288.662	-30.687	18.3	16.1	19.4	7.2	1.5	1.4	-0.005
CENT	288.793	-30.962	19.2	17.9	20.3	9.0	1.5	1.4	-0.001
CFAG	291.767	-31.602	5.6	10.6	6.9	1.4	1.4	1.4	-0.001
CHAN	288.972	-30.897	20.2	17.7	21.3	8.8	1.5	1.4	-0.004
CHAP	289.500	-29.853	15.9	15.7	17.2	6.8	1.5	1.4	0.002
CHIP	288.786	-31.115	21.4	18.8	22.5	9.9	1.7	1.6	-0.002
CHPI ^c	315.015	-22.687	-4.6	10.1	-0.5	-0.8	1.5	1.5	-0.010
CMOR ^a	289.204	-30.205	21.2	15.8	22.4	6.9	2.7	2.2	0.010
COGO	289.025	-31.153	20.0	16.5	21.1	7.6	1.5	1.4	0.000
CONSC	287.588	-35.331	34.9	20.4	35.3	11.7	1.4	1.4	0.001
CONZ ^b	286.975	-36.844	34.9	19.2	35.0	10.5	1.4	1.4	0.001
COPO ^c	289.662	-27.385	21.0	16.6	22.7	7.7	1.8	1.7	0.001
CORD ^a	295.530	-31.528	-2.1	13.1	-0.5	3.5	2.9	2.7	0.003
CTAL	288.330	-30.929	25.0	17.4	26.1	8.6	1.5	1.4	0.000
EALM	288.570	-31.413	27.4	16.7	28.5	7.8	1.5	1.4	0.000
EMAN	288.815	-30.175	15.8	17.3	17.1	8.4	1.5	1.4	0.000
EMAT	288.337	-31.147	28.2	17.4	29.2	8.6	1.5	1.4	-0.005
ESAU	288.316	-30.511	21.0	16.6	22.1	7.8	1.4	1.4	0.000
ESPI	288.545	-31.220	23.2	17.5	24.2	8.7	1.5	1.4	0.000
FORT ^b	321.574	-3.877	-7.0	13.4	-1.9	2.4	1.8	1.5	-0.014
FUND	289.149	-30.383	15.7	16.8	16.9	7.9	1.5	1.4	0.000
GLPS ^c	269.696	-0.743	51.2	10.4	56.3	4.2	1.3	1.3	-0.003
HERA	288.621	-29.998	16.8	17.6	18.0	8.8	1.5	1.4	-0.001
ISPA ^c	250.656	-27.125	67.6	-6.5	67.4	-9.4	0.4	0.3	0.007
KOUR ^b	307.194	5.252	-6.8	13.6	-1.3	3.1	1.0	0.9	0.045
LCAN	288.560	-30.789	22.7	18.0	23.9	9.2	1.7	1.6	-0.001
LHCL ^c	294.405	-38.003	0.3	8.9	0.9	-0.6	1.5	1.4	0.001
LMOL	289.542	-30.742	17.1	15.7	18.3	6.8	1.5	1.4	-0.001
LPER	288.749	-30.365	18.2	19.0	19.4	10.1	1.5	1.4	-0.002
LPGS ^b	302.068	-34.907	-1.6	10.6	0.2	0.5	1.3	1.3	-0.002
LVIL	288.486	-31.909	23.5	16.8	24.5	8.0	1.4	1.4	-0.002
MAUL ^c	289.179	-35.810	20.4	10.2	20.8	1.3	1.6	1.5	0.000
MPAT	288.987	-30.702	18.5	16.1	19.7	7.2	1.5	1.4	0.003
NIPA ^a	288.534	-30.469	22.8	12.5	23.9	3.6	3.8	3.0	0.008
OVEJ	288.806	-31.293	19.5	17.7	20.5	8.8	1.5	1.4	0.000
OVLL ^c	288.796	-30.604	18.8	18.4	19.9	9.5	1.4	1.4	0.000
PACH	288.405	-30.457	21.9	14.1	23.1	5.3	1.6	1.6	0.000
PARA ^c	310.769	-25.448	-1.7	10.6	1.8	-0.1	1.7	1.6	-0.010
PIDN	288.786	-30.815	20.5	17.6	21.6	8.8	1.5	1.4	0.002
POBR	288.496	-30.591	21.3	16.9	22.5	8.1	1.5	1.4	0.000
PTOM	288.428	-31.532	25.5	17.6	26.5	8.8	1.5	1.4	0.001
RIOG ^b	292.249	-53.785	3.4	12.3	1.6	3.0	0.6	0.6	-0.007
SANT ^b	289.331	-33.150	20.4	14.9	21.3	5.9	1.3	1.3	0.000
SJAV ^c	288.267	-35.595	30.3	15.7	30.6	6.9	1.4	1.4	0.001
SLMC ^c	289.037	-31.777	20.1	17.0	21.1	8.1	1.4	1.4	0.000
SPED	288.606	-31.015	19.7	18.5	20.8	9.6	1.5	1.4	0.000
TAHU	288.958	-30.477	16.2	16.2	17.4	7.3	1.5	1.4	-0.003
TOLO ^c	289.194	-30.170	17.3	16.6	18.6	7.6	1.8	1.7	-0.004
TONG	288.498	-30.249	17.5	17.1	18.7	8.3	1.5	1.4	0.000
TUCU ^c	294.770	-26.843	2.9	9.8	5.0	0.3	1.4	1.4	-0.002
VARI ^a	289.250	-30.741	2.1	17.6	3.3	8.7	3.7	3.0	0.011

Latitude and longitude are in decimal degrees. All velocities and velocity uncertainties are in mm/yr.

^a New station measured only twice over a short time period.

^b "Stabilization" station.

^c Permanent station.

Table 3
Nazca/South America relative angular velocities and velocities predicted on the Chilean trench at 31°S using these poles.

	Angular velocity			Predicted velocities	
	Latitude	Longitude	Rotation	Convergence	Azimuth
Nuvel-1A	56.0°N	94.0°W	0.720°/Ma	80 mm/yr	78°N
Larson et al. (1997)	43.8°N	84.8°W	0.740°/Ma	80 mm/yr	81°N
Angermann et al. (1999)	48.8°N	91.7°W	0.590°/Ma	65 mm/yr	77°N
Norabuena et al. (1999)	47.4°N	93.7°W	0.624°/Ma	68 mm/yr	76°N
Sella et al. (2002)	52.1°N	91.2°W	0.633°/Ma	70 mm/yr	79°N
Kendrick et al. (2003) & Brooks et al. (2003)	61.0°N	94.4°W	0.570°/Ma	63 mm/yr	80°N
ITRF2005	53.9°N	87.5°W	0.605°/Ma	67 mm/yr	81°N
This study	55.9°N	95.2°W	0.610°/Ma	68 mm/yr	78°N

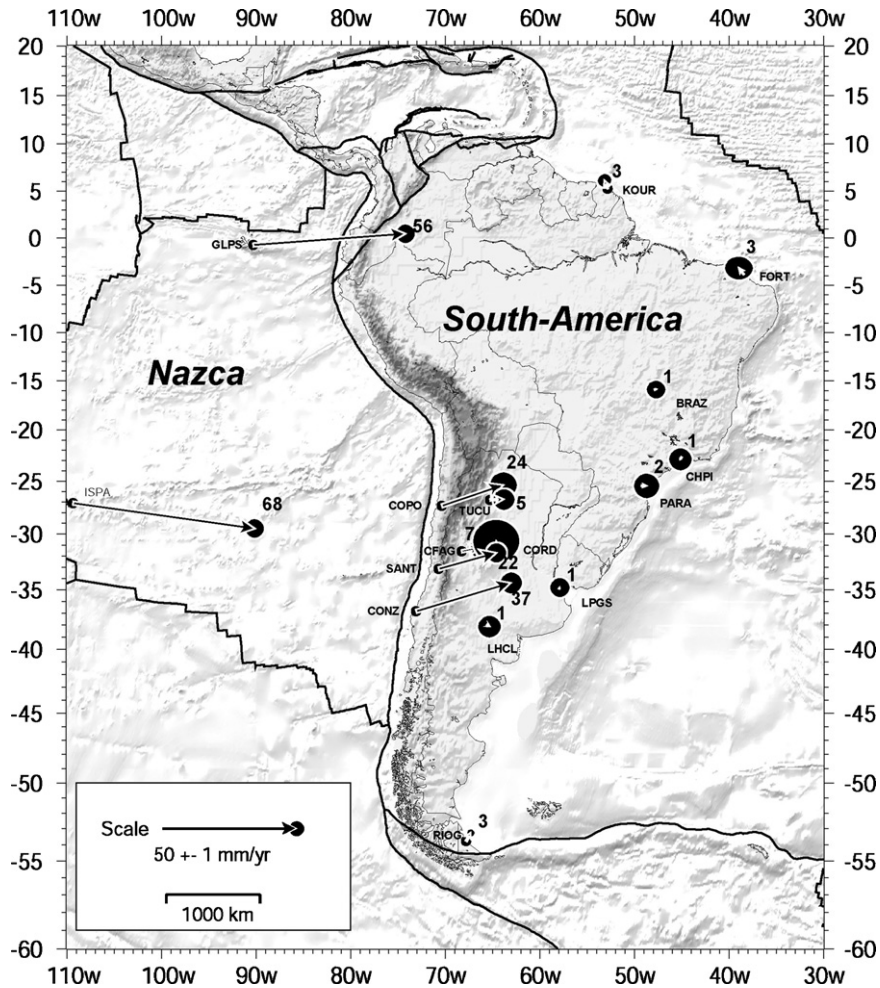


Fig. 3. Large scale network and far field velocities. Dots show locations of GPS stations. Arrows depict their horizontal velocities with respect to a reference frame fixed on the South-America Plate. Bold numbers aside the arrows indicate the velocity in mm/yr. Ellipses depict the region of 99% confidence using the uncertainties in Table 2.

roughly WSW and the velocity at Galapagos Islands (GLPS) is 56 mm/yr oriented West (Fig. 3 and Table 2). These estimates match those of ITRF2000 within 0.5 mm/yr and are significantly smaller than Nuvel-1A predictions for the Nazca plate velocity at those locations. In this study, because we lack a third site near the Eastern boundary of the plate close to the trench, it is not possible to determine whether these differences are due to a reduced angular velocity of the Nazca plate or whether this is due to a significant amount of internal deformation of the plate. However, it is difficult to imagine a mechanism that would stretch the plate and increase near-trench site velocities in order to match the Nuvel-1A prediction of 80 mm/yr of convergence at the trench between the two plates (Table 3). It is also impossible to find an angular velocity which would maintain the Nuvel-1A estimate on the trench and the present day motions observed at ISPA and GLPS. Using ISPA and GLPS velocities we find a pole located very close to Nuvel-1A location (55.9°N and 95.2°W, to compare to 56°N and 95°W) but with a reduced angular rotation about this pole of 0.61°/Myr (compared to 0.72°/Myr) (Table 3). Therefore, and in agreement with previous studies, we conclude that either Nuvel-1A over-estimates Nazca angular velocity by 15% or the plate significantly slowed down since 3 Ma (Norabuena et al., 1999; Angermann et al., 1999; Sella et al., 2002; Kendrick et al., 2003). The Nazca/South America angular velocities found by those previous geodetic studies predict slightly different plate convergence rates at the latitude of our network, but apart from the first one (Larson et al., 1997), they all reach the same order of magnitude (Table 3): the average velocity pre-

dicted on the trench at the latitude of our network is 67 ± 2 mm/yr oriented $78 \pm 3^\circ$ N.

4.2. Central Chile section and Argentina

Deformation along the Chilean trench affects a very wide area including all Chile and penetrating deep into Argentina on the other side of the Andes (see also Brooks et al., 2003). Relative to the South-America plate, CFAG (Coronel Fontana), 400 km from the trench, moves 7 mm/yr inland and TUCU (Tucuman), 550 km from the trench, moves 5 mm/yr also inland. CORD (Cordoba), 700 km from the trench, also has a non-zero residual velocity (4 mm/yr northward) but with a higher uncertainty due to its determination over two epochs spanning a small period of time, so we consider it non-significant (Fig. 4, Table 2). Only LHCL (Lihue Calel), 800 km away from the trench, has a small and insignificant residual velocity (1 mm/yr) and can be located with certainty on the undeformed South-American plate. This pattern is representative of the very far reach of the deformation induced by locking on a low dipping subduction plane (see Section 5).

There is a clear change of trend along the 1100 km length of subduction from 37°S (Concepción) to 27°S (Copiapó). In the south (Concepción–Constitución segment 37–35°S), velocities show a clear rotation pattern from the coast to the Andes. This rotation is accompanied by a decrease of the magnitude of the velocities (37 mm/yr at CONZ and CONS to 21 mm/yr at MAUL). This pattern is well explained by accumulation of elastic deformation in the upper

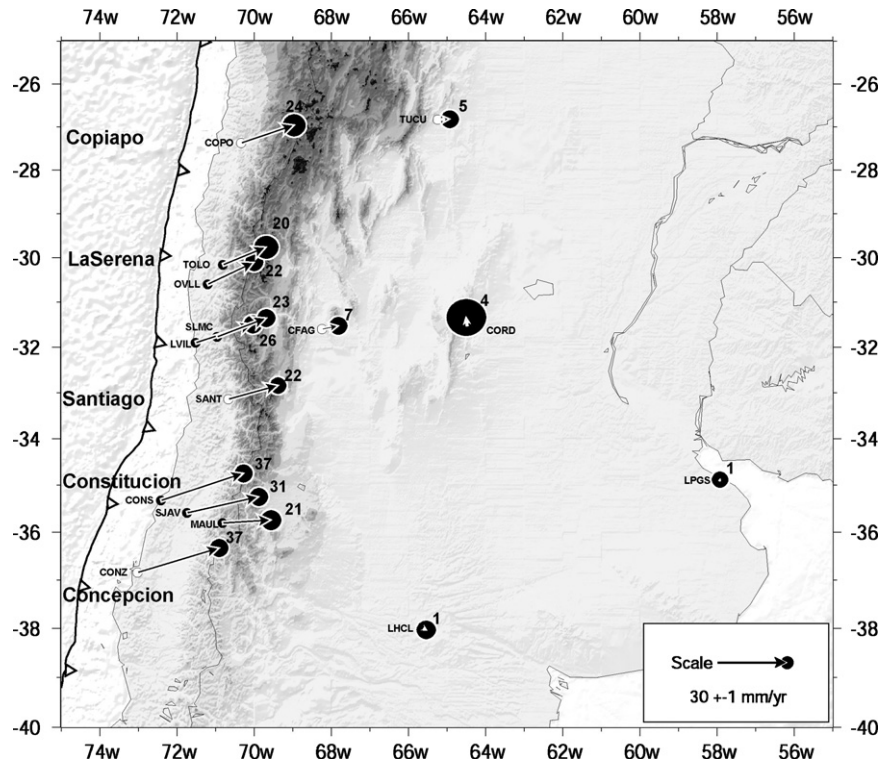


Fig. 4. Central Chile and Argentina section. Dots show locations of GPS stations. Arrows depict their horizontal velocities with respect to a reference frame fixed on the South-America plate. Bold numbers aside the arrows indicate the velocity in mm/yr. Ellipses depict the region of 99% confidence using the uncertainties in Table 2.

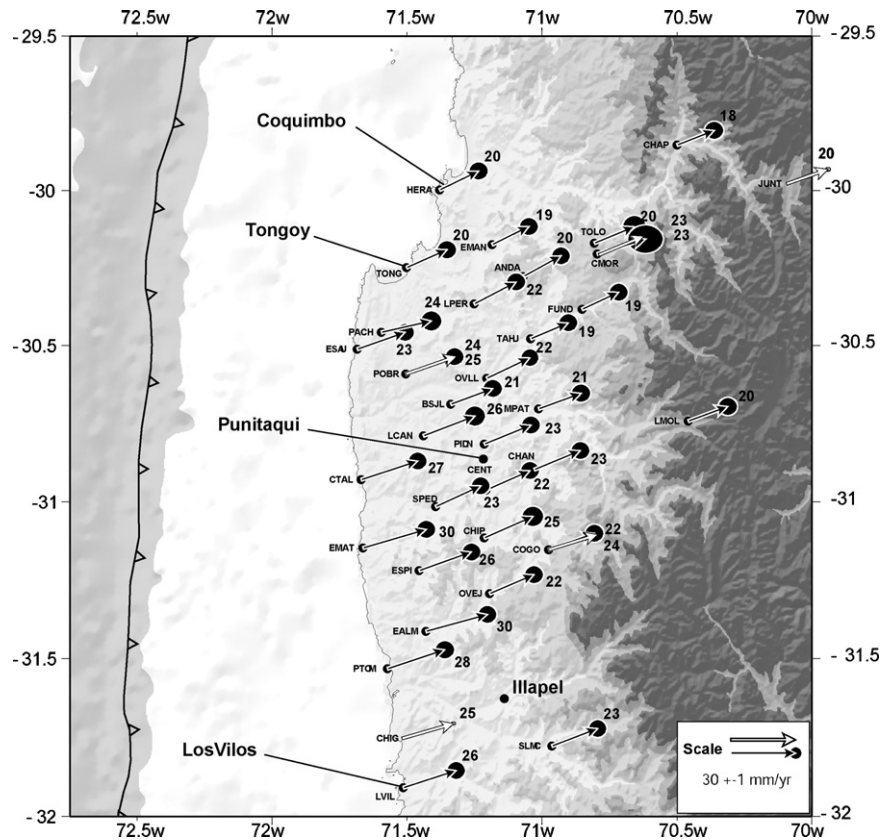


Fig. 5. Coquimbo gap (between 30°S and 32°S). Dots show locations of GPS stations. Arrows depict their horizontal velocities with respect to a reference frame fixed on the South-America plate. Black arrows show our solution, white arrows depict CAP sites velocities of Kendrick et al. (2001), recomputed in ITRF2000. Bold numbers aside the arrows indicate the velocity in mm/yr. Ellipses depict the region of 99% confidence using the uncertainties in Table 2.

plate due to locking on a shallow dipping (15–20°) subduction plane (Ruegg et al., 2002; Ruegg et al., this issue). As we go northward (Coquimbo segment 32–30°S), velocities become parallel and more East–West, whether close to or distant from the trench. More surprisingly, the magnitude of the velocities of coastal stations become smaller: 26 mm/yr at Los Vilos (LVIL – 32°S) compared to 37 mm/yr at Constitución (CONS – 35°S) even-though we are closer to the trench than in the south. This tendency persists at Copiapó (COPO – 27°S) with only 24 mm/yr (Fig. 4, Table 2). Here we use data prior to the seismic swarm of “La Caldera” – 30 April 2006 – during which COPO was displaced ~2 cm westward. These changing velocities are a clear indication of along strike variation of the subduction geometry and/or coupling between the upper and lower plates within the central Chile area.

4.3. Coquimbo gap

In the Coquimbo–Illapel section (30–32°S) the observed velocities differ very much from what is expected from standard elastic modeling. First of all, and unlike in the Concepción–Constitución segment, velocity arrows do not rotate as we move inland. They are aligned almost parallel to each other from the coast to the Andes, striking $70 \pm 5^\circ$ N (Fig. 5, Table 2). Second, and although the trench is only roughly 100 km away from the coast in this area, the amount of compression is much less than in the south: while Andean stations in both segments have roughly the same velocity of 20 mm/yr inland, coastal stations move at 25–30 mm/yr inland in Coquimbo, which should be compared with 40–45 mm/yr around the Arauco peninsula, immediately south of Concepción (37°S) (Ruegg et al., 2002; Ruegg et al., this issue). Finally, there is also a clear change of pattern within the network itself. Coastal stations lying approximately at the same distance from the trench have decreasing velocities as their latitude increase: 30 mm/yr at EMAT (31.1°S),

27 mm/yr at CTAL (30.9°S), and 23 mm/yr at ESAU (30.5°S). In the Andes, stations at corresponding latitudes have approximately the same velocities: 20 mm/yr at LMOL (30.7°S), 20 mm/yr at TOLO (30.2°S) and 18 mm/yr at CHAP (29.9°S). Therefore, it is the amount of compression that is changing (decreasing) with latitude. This decrease is so intense, that North of 30.3°S (Tongoy – TONG) the compression is essentially zero. All stations in this area from the coast to the Andes (TONG, HERA, EMAN, ANDA, TOLO, CHAP) have roughly the same velocity of 18–20 mm/yr. Fig. 6 depicts these tendencies very clearly: strain in the Coquimbo area is on average two times lower than the average strain rate corresponding to the profiles measured between 36°S and 38°S (Ruegg et al., this issue). Moreover, a steady decrease of strain rates with latitude seems to emerge from the picture.

5. Elastic modeling

We assume the upper plate deformation is due to the locking of the subduction interface until a given depth where the slab starts to slip freely. We model this deformation using a simple back-slip assumption for which the inter-seismic accumulation corresponds exactly to the released co-seismic deformation (with reversed sign) (Savage, 1983), and we use Okada’s elastic formulation to relate the surface deformation to the dislocation buried at depth (Okada, 1985). We use a very simple geometry for the dislocation: it is a genuine rectangle with strike and dip angles adjusted to fit the subduction plane in the area. A strike angle of 5° N is given by the average direction of the trench between 30°S and 32°S (Smith and Sandwell, 1997). A dip angle of 10° matches well the interface seismicity between 1963 and 1998 reported by Pardo et al. (2002a). This simple model leaves only two parameters free to invert for a best fit on the observed surface deformation: the locking depth and the amount of “slip” imposed on the locked plane. An obvious value for the slip is the convergence rate between the two plates. However, and this is an important finding, it is simply impossible to fit the data with a plate convergence rate of 65–70 mm/yr. The predicted deformation cannot match the observed one whatever are the locking depth and the dip angle. A reasonable locking depth (>30 km) corresponds to a locked plane large enough to generate twice as much deformation as observed: in that case, coastal velocities cannot be in the range of 20–30 mm/yr. An unrealistic very shallow locking depth (<20 km) can produce such small coastal velocities, but then with the wrong azimuth: the coastline being far East from the longitude reached by the end tip of the (small) locked rectangle, the predicted velocities there already rotated to an almost West–East trend. In summary we need a plane long enough to generate a constant azimuth ($N 70^\circ$) across all Chile, but then we need to reduce the imposed dislocation to reduce the amount of predicted deformation. In other words, the subduction plane in the area cannot be fully locked. The best fit to our data (rms of 2.6 mm/yr) is obtained with a locking depth of 60 km and a dislocation corresponding to 27 mm/yr oriented $N 71^\circ$ (Fig. 7). A slightly better fit (rms = 2.5 mm/yr) can be achieved by adjusting the dip angle to 12° (with locking depth 55 km and 30 mm/yr still oriented $N 72^\circ$). However, as the dip angle increases, the fit on CFAG, the only point constraining the very far field deformation in Argentina, also decreases: a “flat slab” is needed to explain the deformation 500 km away from the trench. A full inversion on all four parameters (dip angle, locking depth, amplitude and orientation of the dislocation) constrains those to dip = $10 \pm 3^\circ$, locking depth = 50 ± 10 km, and convergence = 29 ± 2 mm/yr oriented $71 \pm 2^\circ$.

The latter implies that the upper plate elastic deformation (later described as “slip deficit”) corresponds to only 40–45% of the Nazca–South America convergence rate reported by geodesy, the remaining half being dissipated by free slip. This result is in agreement with the findings of Norabuena et al. (1998) who sug-

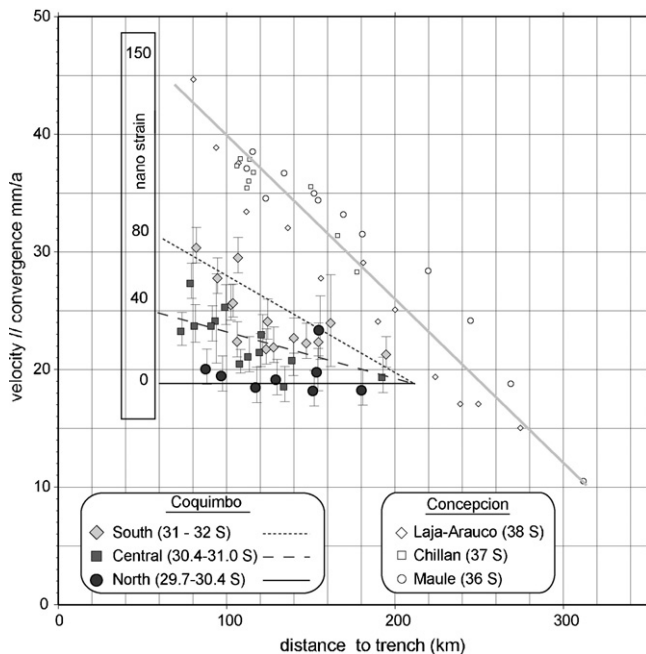


Fig. 6. Comparison of velocity profiles and strain rates at different latitudes. Symbols depict the velocity component parallel to plate convergence (78°) in our region of measurements (black circles north of 30.4° S, grey squares between 30.4° S and 31° S, light grey diamonds south of 31° S), and in the Concepción gap ~1000 km south (open symbols) (Ruegg et al., this issue). Velocities are in mm/yr. The average strain rate at the different latitudes are indicated by the different strain lines: full, dashed, dotted, and grey for Northern part, central part, Southern part of the network, and Concepción network. Strain rates are in nanostrain (10^{-9} yr $^{-1}$).

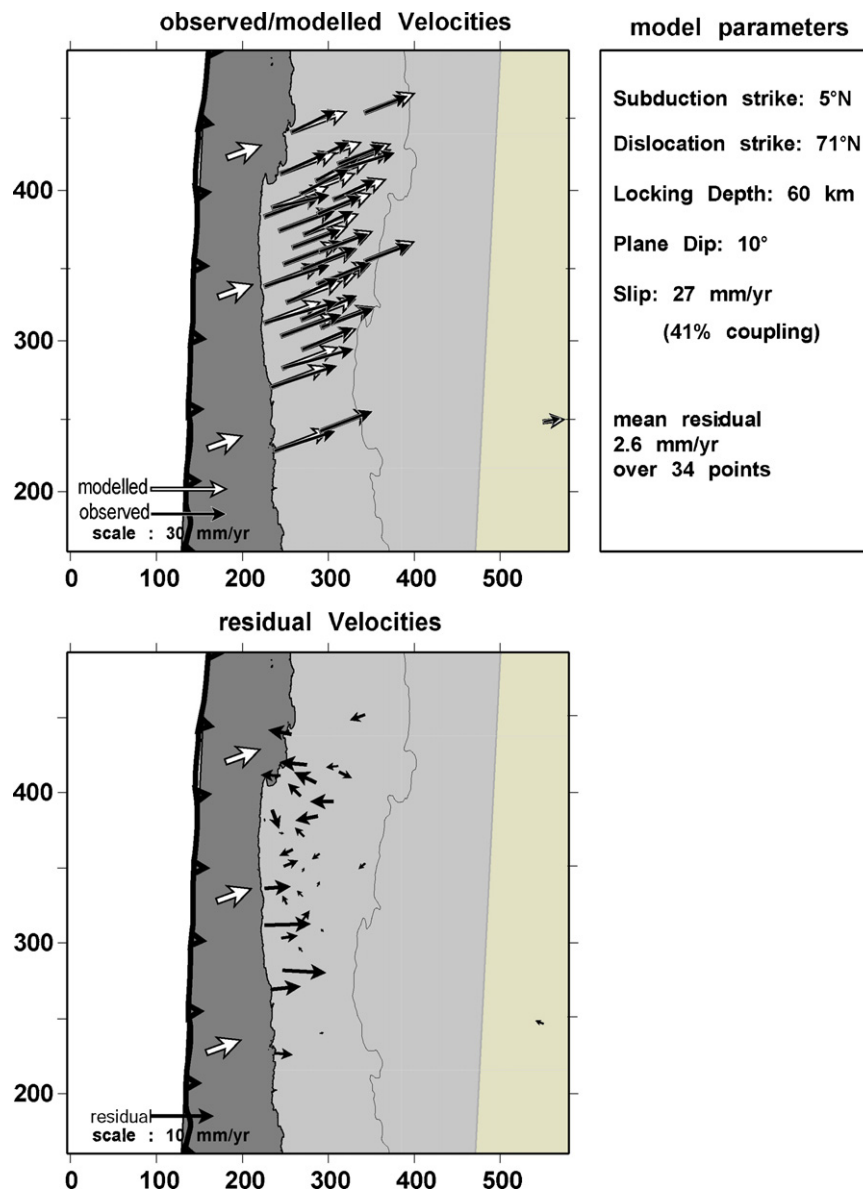


Fig. 7. Elastic modeling of the upper plate deformation in the Coquimbo gap. X- and Y-axis units give UTM coordinates in km. In the upper box, GPS observations (black arrows) and model predictions (white arrows) are shown. In the lower box, residual (i.e. observations–model) velocities are shown (black arrow). In both boxes, the grey shaded rectangles draw the subduction plane buried at depth and the large white arrows depict the dislocation (not to scale) applied on this plane.

gested a coupling of 50% in this area, and contradicts the findings of Klotz et al. (2001), Kendrick et al. (2001), Khazaradze and Klotz (2003) and Brooks et al. (2003) who use 100% coupling and a very shallow locking depth. The small discrepancy between the plate convergence orientation ($78 \pm 3^\circ$) and the azimuth of the best fit dislocation ($71^\circ \pm 2^\circ$) remains unexplained. However, our model clearly shows that it is possible to match the observed deformation with a simple 2-plate model generating elastic deformation of the continental plate. There is no need to introduce a third micro-plate, located between Nazca and South America to account for deformation observed in Argentina (Brooks et al., 2003). On this particular matter, we think the differential motion of 4.5 mm/yr attributed by Brooks et al. (2003) to this micro-plate comes from the convergence deficit introduced by their Nazca–South America angular velocity (Kendrick et al., 2003), which is slower than all other recent geodetic determinations by precisely 4–5 mm/yr (Table 3).

In the first paragraphs, we note the presence of an active seismic swarm over the last decade in the area. In principle, the cumulative co-seismic deformation from the swarm might explain the

relatively low slip deficit we observe and could reconcile the difference with the earlier studies finding a slip deficit of 100%. Using the earthquakes which can be attributed to the subduction interface from the ISC catalog, we find that an equivalent moment of 0.8×10^{20} Nm ($M_w \sim 7.2$) is reached after 15 years (1992–2007). Distributed on a 250-km long segment, with a dip angle of 20° and a locking depth of 50 km (giving a width of 150 km), this corresponds to 5–6 cm of slip. Over 15 years this is 4 mm/yr, and if we concentrate over the last 10 years, that is 5–6 mm/yr of slip deficit. Therefore, a small ($\sim 1/4$ th), although not negligible, part of the 20 mm/yr slip deficit we infer from GPS could be attributed to cumulative co-seismic slip. To get the whole 20 mm/yr, we would need to confine the slip on a smaller portion of the subduction interface: only 15 km depth (i.e. 35 km width). Therefore, we conclude that the bulk of the slip deficit ($\sim 3/4$ th) comes from the modification of the friction properties of the interface in one way or the other and not from co-seismic slip.

This value of 40–45% coupling we obtain is an average value for the whole network. Residual velocities clearly show that lock-

ing has a tendency to be stronger in the south and much weaker in the north where the model over-predicts the observations by 2–5 mm/yr everywhere above 30.5°S (Fig. 7, lower box). In this area, the coupling seems to be essentially zero, all points having the same velocity around 20 mm/yr. This observation may seem inconsistent: if the coupling is permanently zero on the interface, then the strain rate would be low as observe, but the velocities of the coastal sites relative to South America should also be zero. Any motion there would thus be related to the motion of a rigid micro-plate, implying shortening further East, in or on the other side of the Andes. We lack points on the other side of the Andes, in Argentina, to establish a complete profile and determine if the coupling resumes further East (i.e. at greater depth, meaning along dip variations of coupling) and if so at what distance from the trench. In the southern part (32°S) the deformation observed at CFAG matches well the elastic model, but there is no equivalent station at this longitude at 30°S. However, East-West trending strike-slip faulting south of this micro-plate moving 20 mm/yr east should also be observed, because further south the upper plate deformation corresponds to a standard 2-plate model, and this is not the case. Finally, if the subduction interface would slip freely, without imposing any deformation on this part of the upper plate, why would there be any earthquake along this interface in the first place? For these reasons, we conclude that the apparent “zero coupling” in this part of the network can only be a transient feature resulting of competition between elastic deformation due to locking at depth and temporary slip on the interface. Such a feature has already been observed along the Minahassa trench in Sulawesi, Indonesia (Socquet et al., 2006).

Finally, using our procedure, we recomputed the CAP data on five sites within our area of interest. The advantage of doing so is to allow a rigorous mapping in the new ITRF, not available at the time of the CAP campaigns, and therefore a direct comparison with our data in exactly the same reference frame. The velocities we obtain at those points are very close (within 2- σ) to our more recent estimates (Fig. 5, Table 2). This is an indication that our interpretation of a reduced coupling is in fact also compatible with the CAP data. If any difference, our velocities are in general slightly (but marginally) smaller than those measured 10 years ago (–3 mm/yr at MORATOLO, –2 mm/yr at COGO, –1 mm/yr at POBR). This could be an indication of a decrease of the coupling with time, but should be taken with caution given the very small differences.

6. Time variations

Having measured the network already six times, we can establish time series at every benchmark. To do so, we compute stations epoch position by combining daily solutions of each campaign and constraining the reference frame to ITRF2000 using the a-priori positions of the stabilization stations at the time of the campaigns. Every epoch position is assigned a 3- σ uncertainty, where σ is the formal a-priori uncertainty. Then, we project station displacements in the South America reference frame along the average direction of the convergence within the network (N 70°). Over 3 years of measurements, time series look rather linear and there is no indication of any decreasing trend (Fig. 8). If any tendency can be extracted from those time series, it is that stations in the central valley are more “noisy” than stations on the coast or in the mountain. Moreover, this “noise” seems to be correlated, most stations being above or below their linear trend at the same campaigns (Fig. 8, 2nd box). This fact could be an indication of spatially coherent episodes of transient deformation in this area of the network, related to transient slip at depth on the subduction interface. Because those stations are approximately 150 km from the trench, the depth of these transient slip episodes would be around 25 km (using a dip angle of 10°). Such a depth could correspond to the initiation of the

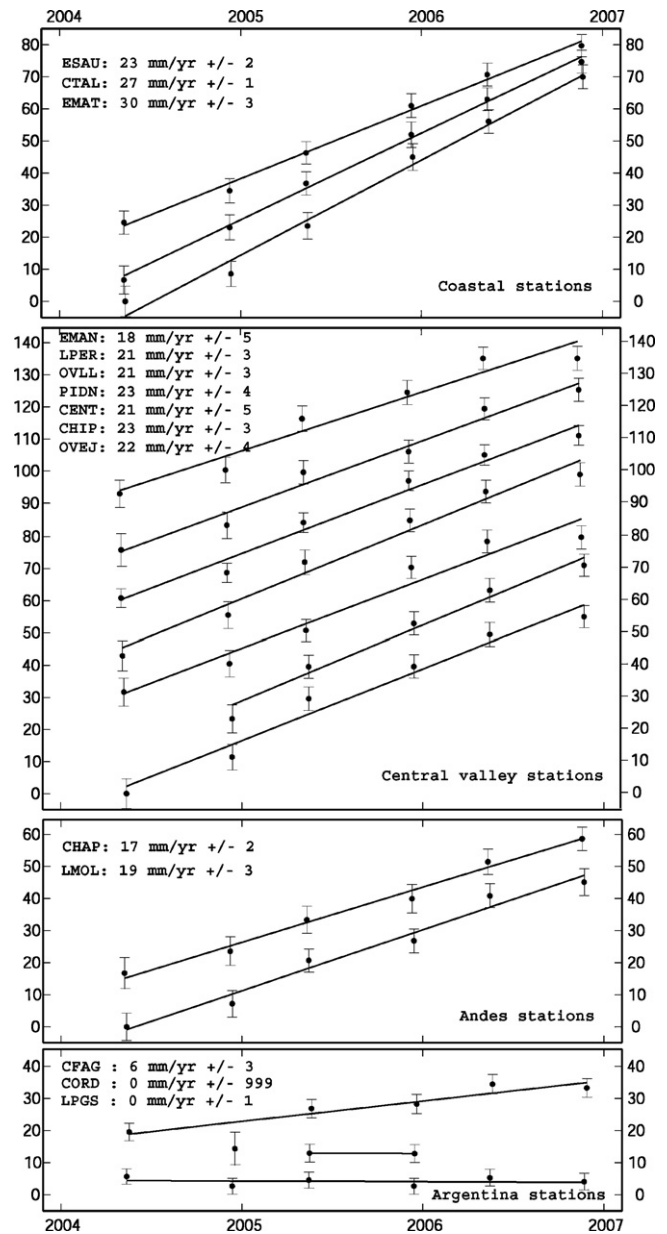


Fig. 8. Sorted time series. Stations horizontal displacements projected along the plate convergence direction (N 70°) and plotted relative to the South-American reference frame. Time is in years and displacements are in mm from an initial arbitrary position. Error bars depict the 3- σ formal error. Time series are plotted in four groups, depending on station distance to the trench: coastal stations (upper box), stations in the Chilean central valley (2nd box), stations in the Chilean side of the Andes (3rd box), and reference stations in Argentina (lower box).

transition zone. Obviously, seasonal variations could also be the origin of correlated noise at a subset of stations. However, it can be noted that that a yearly cycle would not fit well: winter campaigns are sometimes above and some times below the annual trend. Continuous time series over at least 2 or 3 years would be needed to investigate this in detail. For this purpose, we installed 10 cGPS stations in the area, starting in 2006.

7. Conclusion

In this paper, we studied the strain accumulation in the Coquimbo region of North central Chile as this region enters the preparation for a future inter-plate earthquake. The last event in the region occurred 64 years ago, in April 1943 and it was preceded

by another large event in 1880. Seismicity of Coquimbo, as deduced from a study of the ISC catalog, clearly shows acceleration after mid-1998. We cannot resolve yet whether a period of accelerated moment release has started in Coquimbo, but the simultaneous measurement of seismicity and GPS velocities is an obvious approach to better understand the processes that lead to future earthquakes in the region. Comparing the current deformation of the regions of Coquimbo–Illapel and Concepción–Constitución, we observe an apparent weaker strain accumulation in the North than in the South. In general these differences might be related to the geometry variations of the subduction in Central Chile, but we showed that they are mostly related to space and time variations of the coupling. Since the coupling is expected to vary during the seismic cycle, the characterisation of the actual coupling and of its time variations should allow determine at which stage of the seismic cycle this specific segment of the Chilean subduction is. However, we clearly need a longer time span to demonstrate a possible decrease of the coupling with time and quantify it. Transient episodes of slip, possibly related to seismicity on the subduction interface may also have been detected. We are in the process of installing a permanent network of 10–15 cGPS stations in the area to assess whether this process really occurs there and quantify and locate it in the affirmative.

Acknowledgments

We are grateful to many people who participated in measurement campaigns, especially students from DGF and ENS. We thank C. Aranda for his wise advices concerning field measurements. Our geodetic program is sponsored by CNRS/INSU programs (PICS, ACI Catnat), the French National Research Agency (ANR) and by “Nucleo Milenio en Sismotectónica y Peligro Sísmico”. Finally, it contributes to a joint Chilean-French cooperation developed under a University of Chile/CNRS agreement: the International Laboratory (LIA) “Montessus de Ballore”.

References

- Altamimi, Z., Sillard, P., Boucher, C., 2002. ITRF2000: a new release of the international terrestrial reference frame for earth science applications. *J. Geophys. Res.* SA 107 (B10) (art. no. 2214).
- Angermann, D., Klotz, J., Reigber, C., 1999. Space geodetic estimation of the Nazca–South America Euler vector. *Earth Planet. Sci. Lett.* 171, 329–334.
- Barazangi, M., Isacks, B.L., 1976. Spatial distribution of earthquakes and subduction of the Nazca plate beneath South America. *Geology* 4, 686–692.
- Beck, S., Barrientos, S., Kausel, E., Reyes, M., 1998. Source Characteristics of historic earthquakes along the central Chile subduction Zone. *J. South Amer. Earth Sci.* 11, 115–129.
- Beutler, G., Kouba, J., Springer, T., 1993. Combining the orbits of the IGS processing centers. In: Kuba, J. (Ed.), *Proceedings of IGS Analysis Center Workshop*, pp. 20–56.
- Brooks, B.A., Bevis, M., Smalley Jr., R., Kendrick, E., Manceda, R., Lauría, E., Maturana, R., Araujo, M., 2003. Crustal motion in the Southern Andes (26°–36°S): do the Andes behave like a microplate? *Geochem. Geophys. Geosyst.* 4 (10), 1085, doi:10.1029/2003GC000505.
- DeMets, C., et al., 1990. Current plate motions. *Geophys. J. Int.* 101, 425–478.
- DeMets, C., et al., 1994. Effect of the recent revisions to the geomagnetic reversal time scale on estimates of current plate motions. *Geophys. Res. Lett.* 21, 2191–2194.
- Engdahl, E.R., Villaseñor, A., 2002. Global seismicity: 1900–1999. In: Lee, W.H.K., Kanamori, H., Jennings, P.C., Kisslinger, C. (Eds.), *International Handbook of Earthquake and Engineering Seismology*. Academic Press, San Diego, CA.
- Gardi, A.L., Lemoine, A., Madariaga, R., Campos, J., 2006. Modeling of stress transfer in the Coquimbo region of central Chile. *J. Geophys. Res.* 111, B04307, doi:10.1029/2004JB003440.
- Herring, T.A., et al., 1990. Geodesy by radio astronomy: the application of Kalman filtering to very long baseline interferometry. *J. Geophys. Res.* 95 (12), 561–562, 581.
- International Seismological Centre, 2001. On-line Bulletin. <http://www.isc.ac.uk>. Internat. Seis. Cent., Thatcham, United Kingdom.
- Kelleher, J., 1972. Rupture zones of large South American earthquakes and some predictions. *J. Geophys. Res.* 77, 2087–2103.
- Kendrick, E., Bevis, M., Smalley, R., Brooks, B., 2001. An integrated crustal velocity field for the central Andes. *Geochem. Geophys. Geosyst.* 2.
- Kendrick, E., Beavis, M., Smalley, R., Brooks, B., Barriga-Vargas, R., Lauria, E., Souto-Forbes, L.P., 2003. The Nazca–South America Euler vector and its rate of change. *J. South Amer. Earth Sci.* 16, 125–131.
- Khazaradze, G., Klotz, J., 2003. Short and long-term effects of GPS measured crustal deformation rates along the South-Central Andes. *J. Geophys. Res.* 108 (B4), 1–13.
- King, R.W., Bock, Y., 2000. Documentation for the GAMIT GPS software Analysis Version 9.9. Mass. Inst. of Technol., Cambridge.
- Klotz, J., Khazaradze, G., Angermann, D., Reigber, C., Perdomo, R., Cifuentes, O., 2001. Earthquake cycle dominates contemporary crustal deformation in Central and Southern Andes. *Earth Planet. Sci. Lett.* 193, 437–446.
- Larson, K., Freymuller, J.T., Philippsen, S., 1997. Global consistent rigid plate velocities from GPS. *J. Geophys. Res.* 102, 9961–9981.
- Lemoine, A., Madariaga, R., Campos, J., 2001. Evidence for earthquake interaction in central Chile: the July 1997–September 1998 sequence. *Geophys. Res. Lett.* 28, 2742–2746.
- Mignan, A., Bowman, D.D., King, G.C.P., 2006. An observational test of the origin of accelerating moment release before large earthquakes. *J. Geophys. Res.* 111, B11304, doi:10.1029/2006JB004374.
- National earthquake information center, 2006. On line catalogs, <http://neic.usgs.gov/neis/epic/>.
- Neilan, R., 1995. The evolution of the IGS global network, current status and future aspects. In: Zumberge, J.F., et al. (Eds.), *IGS Annual Report*. JPL Publ., pp. 95–18, 25–34.
- Nishenko, R., 1985. Seismic potential for large and great intraplate earthquakes along the Chilean and Southern Peruvian margins of South America: a quantitative reappraisal. *J. Geophys. Res.* 90, 3589–3615.
- Norabuena, E., Leffler-Griffin, L., Mao, A., Dixon, T., Stein, S., Sacks, S.I., Ocola, L., Ellis, M., 1998. Space Geodetic observations of Nazca–South America convergence across the central Andes. *Science* 270, 358–362.
- Norabuena, E., Dixon, T., Stein, S., Harrison, C.G.A., 1999. Decelerating Nazca–South America and Nazca–Pacific Plate Motion. *Geophys. Res. Lett.* 26, 3405–3408.
- Okada, Y., 1985. Surface deformation due to shear and tensile faults in a half-space. *Bull. Seism. Soc. Am.* 75, 1135–1154.
- Pardo, M., Comte, D., Monfret, T., 2002a. Seismotectonic and stress distribution in the central Chile subduction zone. *J. S. Am. Earth Sci.* 15, 11–22.
- Pardo, M., Comte, D., Monfret, T., Boroschek, R., Astroza, M., 2002b. The October 15, 1997 Punitaqui Earthquake (Mw = 7.1): a destructive event within the subducting Nazca plate in central Chile. *Tectonophysics* 345, 199–210.
- Ruegg, J.C., Campos, J., Madariaga, R., Kausel, E., DeChabaliere, J.B., Armijo, R., Dimitrov, D., Georgiev, I., Barrientos, S., 2002. Interseismic strain accumulation in south central Chile from GPS measurements, 1996–1999. *Geophys. Res. Lett.* 29 (11), doi:10.1029/2001GL013438.
- Savage, J.C., 1983. A dislocation model of strain accumulation and release at a subduction zone. *J. Geophys. Res.* 88, 4948–4996.
- Sella, G.F., Dixon, T.H., Mao, A., 2002. REVEL: a model for recent plate velocities from space geodesy. *J. Geophys. Res.* 107 (B4), 10.1029.
- Smith, W., Sandwell, D., 1997. Global sea floor topography from satellite altimetry and ship depth soundings. *Science* 277, 1956–1962.
- Socquet, A., Simons, W., Vigny, C., McCaffrey, Ambrosius, B., Spakman, W., Subarya, C., Sarsito, D., 2006. Kinematic behaviour, crustal block rotations and plate coupling in the triple junction area in SE Asia from inversion of GPS and slip vector data (Sulawesi, Indonesia). *J. Geophys. Res.* 111, B08409, doi:10.1029/2005JB003963.